Correlating Sulfur Reactivity of PtxPd1−x Nanoparticles with a Bimetallic Interaction Effect

ARTICLE *in* THE JOURNAL OF PHYSICAL CHEMISTRY C · JUNE 2011

Impact Factor: 4.77 · DOI: 10.1021/jp200182a

5 AUTHORS, INCLUDING:

Fabiano Bernardi
Universidade Federal do Rio Grande do Sul
25 PUBLICATIONS **289** CITATIONS

SEE PROFILE

Luca Olivi
Sincrotrone Trieste S.C.p.A.
77 PUBLICATIONS **1,250** CITATIONS

SEE PROFILE

THE JOURNAL OF PHYSICAL CHEMISTRY C

ARTICLE

pubs.acs.org/JPCC

Correlating Sulfur Reactivity of Pt_xPd_{1-x} Nanoparticles with a Bimetallic Interaction Effect

Fabiano Bernardi,[†] Agnès Traverse,[‡] Luca Olivi,[§] Maria C. M. Alves,[∥] and Jonder Morais*[,†]

[†]Laboratório de Espectroscopia de Elétrons (LEe$^-$), Instituto de Física, Universidade Federal do Rio Grande do Sul (UFRGS), Avenida Bento Gonçalves, 9500, Bairro Agronomia, CP 15051, CEP 91501-970, Porto Alegre, RS, Brazil

[‡]Laboratoire de Chimie-Physique, UMR8000, Université de Paris-Sud, Bât. 349, 91405 Orsay, France

[§]Sincrotrone Trieste, Strada Statale 14 - km 163.5, 34149 Basovizza, Trieste, Italy

[∥]Instituto de Química, Universidade Federal do Rio Grande do Sul (UFRGS), Avenida Bento Gonçalves, 9500, Bairro Agronomia, CP 15003, CEP 91501-970, Porto Alegre, RS, Brazil

ABSTRACT: Pt_xPd_{1-x} (x = 0.5, 0.3, or 0) nanoparticles submitted to hydrogen reduction and posterior H_2S sulfidation at 300 °C were characterized by in situ and ex situ X-ray absorption spectroscopy (XAS). The XAS measurements allowed monitoring short-range order changes around the Pt and Pd atoms induced by the thermal processes. Using the structural parameters obtained from the fitting procedure of the extended X-ray absorption fine structure (EXAFS) data, it was observed that the number of chemisorbed sulfur atoms is proportional to the quantity of Pd in the vicinity of Pt. A correlation between the sulfur reactivity of the nanoparticles and the bimetallic interaction effect is then evidenced.

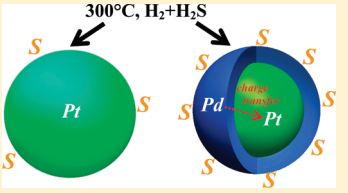

1. INTRODUCTION

Considerable attention has been paid recently toward the development of catalysts with high activity for the hydrogenation of aromatics (HYD) and hydrodesulfurization (HDS) reactions. Such studies indicate that particulate emissions in diesel exhaust gases can be reduced by decreasing the fuel's sulfur content. A few highly active systems for the HYD have already been obtained, although they are very susceptible to sulfur poisoning.[1] Thus, the use of these catalysts is still limited by severe pretreatment requirements until sulfur tolerance can be greatly improved.

Since the mechanism of metal poisoning by sulfur compounds involves strong chemisorption of the S-containing molecule on the metal sites, followed by its hydrogenolysis, as represented by $Me^0 + H_2S \leftrightarrow Me{-}S + H_2$, the resulting H_2S may lead to the formation of a stable and inactive Me−S species on the catalyst's surface.[2] However, this equilibrium may shift to the left-hand side when hydrogen pressure is high, and/or when the physicochemical characteristics of the metal atoms are modified.

It is well-known[3,4] that the main approach to improve sulfur resistance of noble metal-based catalysts used in the HYD reaction is to modify the metal atom's electronic properties by using acidic supports such as γ-Al_2O_3[5,4] and zeolites.[6,7] The model that has been introduced to explain the uncommon behavior of noble metals on acidic sites accounts for its electron deficient character. In the case of Pt- based catalysts, the chemical interaction between the strong acid support and the Pt atoms induces an electron-deficient character at the metal. The partial positive charge on Pt decreases the bond strength between the electron acceptor (S) and the electron-deficient metal (Pt), which improves the sulfur resistance of the catalyst.[8−10]

Another approach to lower the sulfur poisoning of a noble metal catalyst is to alloy the active component with another metal.[11] Bimetallic systems enable the tailoring of catalytic activity and selectivity, which is referred to in the literature as occurring through a "cooperative effect".[12,13] For example, in a sulfur-containing atmosphere, Pt−Pd catalysts were reported to be more sulfur resistant than either pure Pd or pure Pt catalysts.[14,15] Sulfur tolerance of the bimetallic Pt−Pd catalysts is influenced by several factors, the main ones being the sample preparation details,[16] degree of Pt−Pd alloy formation (ensemble and electronic effects),[2,17,11] Pt−Pd particle sizes,[18] and interaction between the Pt−Pd nanoparticles and the support.[8,19,7] The ensemble effect[17] occurs when the addition of a second metal changes the distribution of active sites, altering the reaction pathways. The presence of atoms of the second metal around Pt active sites may block sulfur adsorption on Pt. The electronic effect can be explained by the formation of electron-deficient Pt resulting from charge transfer in bimetallic Pt−Pd systems.[11,2] Navarro et al.[2] showed strong Pt−Pd interaction in bimetallic Pt−Pd/SiO_2−Al_2O_3 particles. From a structural analysis of the catalysts, the authors indicated that the electron-deficient character of Pt was responsible for the strong sulfur resistance of the Pt−Pd catalysts.

Therefore, one may assume that electron-deficient species in Pt−Pd systems are formed either by the interaction of the metal and acid sites of the support or by charge transfer between the Pt and Pd atoms.

In a recent work,[20] we used in situ X-ray absorption spectroscopy (XAS) to study nonsupported Pt_xPd_{1-x} (x = 1, 0.7, or 0.5) nanoparticles under hydrogen reduction and posterior sulfidation. The Pt L_3 edge was monitored, and we observed that the

Received: January 7, 2011
Revised: May 5, 2011
Published: June 03, 2011

dx.doi.org/10.1021/jp200182a | J. Phys. Chem. C 2011, 115, 12243–12249

reduction process is a necessary step prior to the occurrence of any sulfur reaction and that Pd migrates toward the surface, forming a Pt-rich core−Pd-rich shell structure.

In the present study, we have extended our investigation to systems with higher contents of Pd, i.e., nonsupported Pt_xPd_{1-x} (x = 0.5, 0.3 or 0) nanoparticles. They were also submitted to hydrogen reduction and posterior H_2S sulfidation at 300 °C and characterized by XAS at both Pt L_3 and Pd K edges. The use of nonsupported catalysts, instead of catalysts supported on zeolites or γ-Al_2O_3, allows one to evidence any interaction between Pt and Pd. The atom-specific short-range order investigation by XAS provides a way of monitoring local structural changes induced by reduction and sulfidation processes. Using the structural parameters obtained from the fitting procedure of the extended X-ray absorption fine structure (EXAFS) oscillations, we searched for a correlation between the sulfur reactivity of the nanoparticles and the bimetallic interaction effect. We report on the results of ex situ and in situ XAS measurements for a new range of alloy composition, completing the ones investigated in a previous study.[20] The overall results allow sustaining the model for the bimetallic interaction effect that we propose in the present study.

2. EXPERIMENTAL METHODS

2.1. Preparation of the Nanoparticles. Pt_xPd_{1-x} nanoparticles were prepared by dissolution of the Pt and Pd precursors, $Pt_2(dba)_3$ and $Pd(acac)_2$, in 1 mL of 1-*n*-butyl-3-methylimidazolium hexafluorophosphate ($BMIPF_6$). The resulting solution was reacted with molecular hydrogen at 75 °C and 4 atm for 5 min.[21] At the end of the process, a black solution was formed and the nanoparticles were isolated by centrifugation.

2.2. Transmission Electron Microscopy (TEM) Measurements. TEM analyses were carried out on an electron microscope operating at an accelerating voltage of 80 kV (JEOL JEM-1200 EXII). For these measurements, a drop of the dispersed Pt_xPd_{1-x} nanoparticles was spotted on a holey carbon-coated copper grid. The images were analyzed using the Scan Sigma Pro 5.0 software from which the histogram of size distribution was obtained.

2.3. XAS Measurements. Ex situ XAS measurements were collected at both the Pt L_3 edge and the Pd K edge, while the in situ XAS experiments monitored only the Pt L_3 edge.

Approximately 10 mg of the Pt_xPd_{1-x} (x = 0.5, 0.3, or 0) nanoparticle powder was compacted to produce 5 mm diameter pellets. For the ex situ measurements, one pellet at a time was introduced to the previously described reactor,[22] which allows for controlled thermal treatment of the sample under controlled gas flow. Each sample pellet was submitted to reduction and sulfidation processes under gaseous environment. For these experiments, the nanoparticles were reduced at 300 °C for 2 h 20 min under 95% He + 5% H_2 flux and then exposed to the sulfidation process by a flux of 95% He + 5% H_2S for 2 h 20 min. The total gas pressure at the sample was kept at approximately 35 psi. Ex situ XAS spectra were measured on the as-prepared, reduced, and sulfided samples. These measurements were performed in transmission mode at the ELETTRA Synchrotron Light Source at the XAFS beamline. The Pt L_3 edge and Pd K edge spectra were collected using a Si (311) crystal and three ionization chambers, and all measurements were taken at room temperature. Standard Pt and Pd foils were used to calibrate the monochromator. The spectra were acquired in the range of 11450−12400 eV with a 2 eV step and 2s/point for the Pt L_3 edge, and 24150−25400 eV with a 2 eV step and 1s/point for the Pd K edge. Two to four scans were collected in order to improve the signal-to-noise ratio.

In situ XAS measurements were performed in transmission mode at the LNLS (Brazilian Synchrotron Light Laboratory) at the XAFS1 beamline.[23] Each sample pellet of the Pt_xPd_{1-x} (x = 0.5 and 0.3) nanoparticles was introduced into the dedicated reactor.[22] The samples were then submitted to the same reduction and sulfidation processes described above, and the spectra were acquired in situ and at the end of each process, i.e., after reduction and sulfidation at 300 °C in the presence of a H_2 or H_2S containing atmosphere, respectively. The XAS spectra were collected at the Pt L_3 edge using a channel-cut Si (111) crystal and three argon-filled ionization chambers. A standard Pt foil was used to calibrate the monochromator. The spectra were acquired in the range of 11440−12200 eV with a 2 eV step and 2s/point, and two to four scans were collected in order to improve the signal-to-noise ratio.

2.4. Data Analysis. The XAS spectra were analyzed in accordance with the standard procedure of data reduction,[24] using IFEFFIT.[25] FEFF was used to obtain the phase shift and amplitudes.[26] The EXAFS signal $\chi(k)$ was extracted and then Fourier transformed (FT) using a Kaiser-Bessel window with Δk range of 8.4 $Å^{-1}$ and 8.0 $Å^{-1}$ for Pt L_3 and Pd K edges, respectively. To obtain the phase shift and amplitudes, a cluster of atoms with 10 Å radius was built considering the face-centered cubic (fcc) crystal structure of Pd. For the bimetallic nanoparticles, Pd atoms were randomly replaced by Pt atoms respecting the composition of the nanoparticles (x values). Single and multiple scattering events were considered in the fitting procedure. All the presented fittings of the absorption data were k^2-weigthed. During the EXAFS fitting, the number of free parameters (used as variables in the fitting procedure) was always lower than the number of independent ones. The amplitude reduction term (S_0^2) value was fixed at 0.84 (Pt absorber) and 0.82 (Pd absorber) for all samples, which was obtained from the fitting of standard Pt and Pd foil spectra and, in some cases, it was necessary to apply cumulant expansion (c_3 and c_4 values around 10^{-4}).

3. RESULTS

The ex situ EXAFS spectra at the Pt L_3 edge for bimetallic nanoparticles $Pt_{0.5}Pd_{0.5}$ and $Pt_{0.3}Pd_{0.7}$ were collected for the as-prepared, reduced, and sulfided samples. The EXAFS signals $\chi(k)$ and the FTs are presented in Figure 1, as well as the best fit of the signal (gray lines). The measurement of a standard Pt foil is also included.

The EXAFS signals for the as-prepared samples (Figure 1a) are similar to those of bulk Pt, where the characteristic signature of the fcc structure can be found for the nanoparticles. The overall shape is identical to bulk Pt with a damping of the oscillations that is clearly seen for $k > 5$ $Å^{-1}$. The damping could be due to particle structural disorder and (or) size reduction, as explained in our previous study.[20] The FTs (Figure 1a) have two peaks in the 2−3 Å range (uncorrected from the phase shift) that are associated with Pt−Pt and Pt−Pd bonds in the coordination shell. The absence of contributions at greater distances indicates only short-range order in the nanoparticles. No significant change is seen in the position of the peaks with the Pd content. For $Pt_{0.5}Pd_{0.5}$ there is a peak at about 1.5 Å (uncorrected from the phase shift) that corresponds to a bond of Pt with a light element.

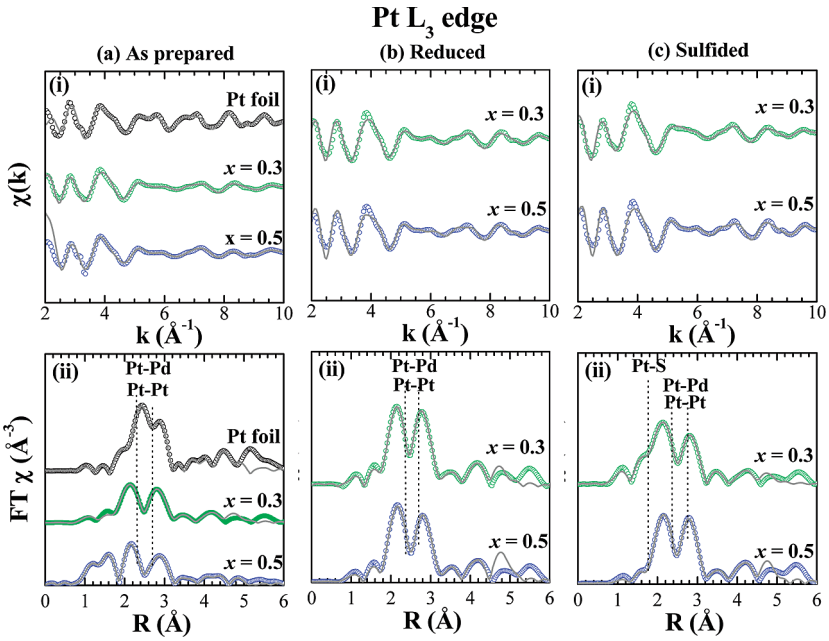

Figure 1. (i) EXAFS signals at the Pt L_3 edge for the Pt_xPd_{1-x} nanoparticles for different x values and (ii) the corresponding FT for the (a) as-prepared, (b) reduced at 300 °C, and (c) sulfided at 300 °C. The points represent the experimental data, and the gray lines are the fitting results.

After reduction, the FTs of both samples are quite similar, and for $Pt_{0.5}Pd_{0.5}$ the peak at 1.5 Å disappears (Figure 1b). The effect of the sulfidation is hardly seen in the EXAFS signals (Figure 1c). However, the FTs show that $Pt_{0.3}Pd_{0.7}$ presents some degree of sulfidation, as observed by the asymmetry in the first peak of the FT, which corresponds to Pt−S bonds.[20] For $Pt_{0.5}Pd_{0.5}$, the contribution of the Pt−S bond is not clearly observed.

The quantitative analysis extracted from the EXAFS data is presented in Table 1 and yielded typical R-factors between 0.002 and 0.01, illustrating the good fit quality. For all the as-prepared samples, the metal−metal distances (Pt−Pt = 2.74 Å and Pt−Pd = 2.76 Å) are close to those of an fcc lattice and match, within the acceptable range of uncertainty, that of pure fcc Pt. The coordination number values (N) from the EXAFS results for the as-prepared samples are in agreement with the TEM (transmission electron microscopy) findings, since the coordination number can be related to the average nanoparticle diameter.[27] Table 2 compares the values of the mean diameter obtained by EXAFS analysis and TEM. TEM results of the Pt_xPd_{1-x} nanoparticles show that their mean diameter is not strongly dependent on the Pt composition (x) over the entire composition interval ($0 < x < 1$). This diminishes any nanoparticle size effect on the sulfur tolerance[18] in the present study. A typical TEM image is shown in Figure 2 for the $Pt_{0.3}Pd_{0.7}$ nanoparticles along with their size distribution, where the gray objects correspond to Pt−Pd nanoparticles and the darker ones correspond to nanoparticles' superposition.

After reduction, $Pt_{0.5}Pd_{0.5}$ nanoparticles display a significant bond contraction, but the $Pt_{0.3}Pd_{0.7}$ nanoparticles do not present any change in the bond length (Table 1). The sulfur reactivity of the nanoparticles can be observed in the coordination numbers obtained for the Pt−S bond. No sulfur bond is present for the $Pt_{0.5}Pd_{0.5}$ while, for the $Pt_{0.3}Pd_{0.7}$ nanoparticles, it is necessary to include a Pt−S contribution with a coordination number of 1.1 ± 0.1 at 2.21 ± 0.02 Å.

Figure 3 shows the $\chi(k)$ signal and the FT for the as-prepared, reduced, and sulfided $Pt_{0.5}Pd_{0.5}$, $Pt_{0.3}Pd_{0.7}$, and Pd nanoparticles

Table 1. Ex Situ XAS Measurements at the Pt L_3 Edge: Results Obtained from the Quantitative Analysis of the EXAFS Data for the Coordination Shell Yielding the Coordination Number (N), Distance (R) and Debye Waller Factor (σ^2) for the As-Prepared, Reduced (T = 300 °C), and Sulfided (T = 300 °C) Samples

x	pair	N	R (Å)	σ^2 (10^{-2} Å^2)
		As-Prepared		
0.5	Pt−Pt	6.9 ± 0.6	2.74 ± 0.02	(0.55 ± 0.05)
	Pt−Pd	3.9 ± 0.3	2.76 ± 0.02	(0.46 ± 0.04)
0.3	Pt−Pt	6.3 ± 0.2	2.74 ± 0.02	(0.45 ± 0.03)
	Pt−Pd	4.0 ± 0.1	2.73 ± 0.02	(0.47 ± 0.03)
		Reduced		
0.5	Pt−Pt	5.1 ± 0.1	2.71 ± 0.02	(0.20 ± 0.02)
	Pt−Pd	4.0 ± 0.1	2.71 ± 0.02	(0.20 ± 0.02)
0.3	Pt−Pt	6.0 ± 1	2.73 ± 0.02	(0.40 ± 0.1)
	Pt−Pd	5.0 ± 0.1	2.74 ± 0.02	(0.50 ± 0.02)
		Sulfided		
0.5	Pt−S	0.0		
	Pt−Pt	6.7 ± 0.2	2.74 ± 0.02	(0.40 ± 0.01)
	Pt−Pd	4.7 ± 0.1	2.74 ± 0.02	(0.40 ± 0.01)
0.3	Pt−S	1.1 ± 0.1	2.21 ± 0.02	(0.70 ± 0.1)
	Pt−Pt	5.7 ± 0.2	2.74 ± 0.02	(0.22 ± 0.02)
	Pt−Pd	3.1 ± 0.1	2.73 ± 0.02	(0.24 ± 0.02)

Table 2. Comparison of the As-Prepared Nanoparticle's Mean Diameter Values Obtained from the Pt L_3 Edge EXAFS Analysis (D_{XAS}) and TEM (D_{TEM})

x	D_{XAS} (nm)	D_{TEM} (nm)
0.5	5.0 ± 0.5	4.5 ± 0.7
0.3	4.0 ± 0.3	4.0 ± 0.8

dx.doi.org/10.1021/jp200182a |J. Phys. Chem. C 2011, 115, 12243–12249

measured ex situ at the Pd K edge. Measurements of a standard Pd foil and PdS are also included. The results of the as-prepared and reduced samples do not present any significant modification for the different compositions (Figures 3a,b). In contrast, the comparison of the sulfided samples (Figure 3c) shows stronger changes for Pd and $Pt_{0.3}Pd_{0.7}$ nanoparticles, while the $Pt_{0.5}Pd_{0.5}$ nanoparticles remain almost unchanged. The FT of $Pt_{0.3}Pd_{0.7}$ has a stronger contribution at $R = 2.3$ Å (uncorrected from the phase shift) due to Pd−S bonds, suggesting a higher degree of sulfidation for this composition.

Table 3 presents the quantitative parameters obtained from the EXAFS adjustment at the Pd K edge. Typical R-factors were between 0.003 and 0.017, illustrating good fit quality.

The reactivity with sulfur is reflected on the coordination numbers obtained for the Pd−S pair: (0.6 ± 0.3) for $Pt_{0.5}Pd_{0.5}$, (1.7 ± 0.1) for $Pt_{0.3}Pd_{0.7}$, and (0.7 ± 0.1) for Pd nanoparticles. The mean metal−metal distances are close to those of pure fcc Pd. For the bimetallic samples, the coordination number for Pd−Pt pair contribution (N_{Pd-Pt}) decreases after the sulfidation process, and for the $Pt_{0.3}Pd_{0.7}$ case, it is remarkable that $N_{Pd-Pt} = 0$. These observations corroborate the atomic rearrangement in nonsupported Pt_xPd_{1-x} nanoparticles that induces the formation of a core−shell structure, with a Pd-enriched shell and a Pt-rich

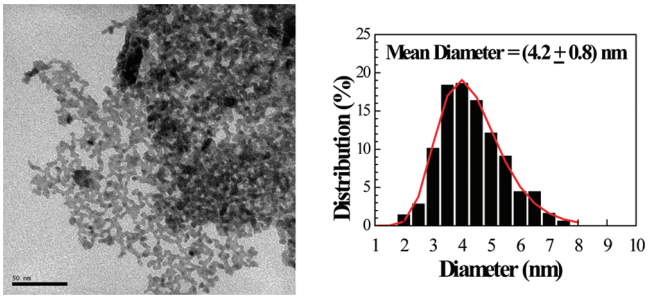

Figure 2. TEM image for the $Pt_{0.3}Pd_{0.7}$ nanoparticles along with the size distribution. The solid line in the histogram represents the monomodal function used to adjust the diameter distribution. The scale bar dimension is 50 nm.

Table 3. Ex Situ XAS Measurements at the Pd K Edge: Results Obtained from the Quantitative Analysis of the EXAFS Data for the Coordination Shell Yielding the Coordination Number (N), Distance (R) and Debye Waller Factor (σ^2) for the As-Prepared, Reduced (T = 300 °C), and Sulfided (T = 300 °C) Samples

x	pair	N	R (Å)	σ^2 (10^{-2} Å^2)
		As-Prepared		
0.5	Pd−Pd	7.2 ± 0.3	2.78 ± 0.02	0.30 ± 0.05
	Pd−Pt	4.1 ± 0.3	2.76 ± 0.03	0.19 ± 0.06
0.3	Pd−Pd	9.1 ± 0.3	2.72 ± 0.02	0.62 ± 0.03
	Pd−Pt	2.6 ± 0.4	2.72 ± 0.02	0.3 ± 0.1
0	Pd−Pd	10.2 ± 0.2	2.74 ± 0.02	0.57 ± 0.02
		Reduced		
0.5	Pd−Pd	6.7 ± 0.2	2.76 ± 0.02	0.21 ± 0.02
	Pd−Pt	4.6 ± 0.2	2.80 ± 0.02	0.43 ± 0.02
0.3	Pd−Pd	8.7 ± 0.1	2.75 ± 0.02	0.57 ± 0.01
	Pd−Pt	3.0 ± 0.2	2.75 ± 0.02	0.57 ± 0.01
0	Pd−Pd	10.8 ± 0.3	2.74 ± 0.02	0.61 ± 0.02
		Sulfided		
0.5	Pd−S	0.6 ± 0.3	2.26 ± 0.02	0.8 ± 0.2
	Pd−Pd	8.4 ± 0.2	2.77 ± 0.02	0.21 ± 0.02
	Pd−Pt	4.0 ± 0.3	2.81 ± 0.02	0.36 ± 0.07
0.3	Pd−S	1.9 ± 0.1	2.31 ± 0.02	0.25 ± 0.05
	Pd−Pd	3.4 ± 0.2	2.80 ± 0.02	0.51 ± 0.04
	Pd−Pt	0.0	---	---
0	Pd−S	0.7 ± 0.1	2.30 ± 0.02	0.7 ± 0.1
	Pd−Pd	3.9 ± 0.1	2.74 ± 0.02	0.53 ± 0.02

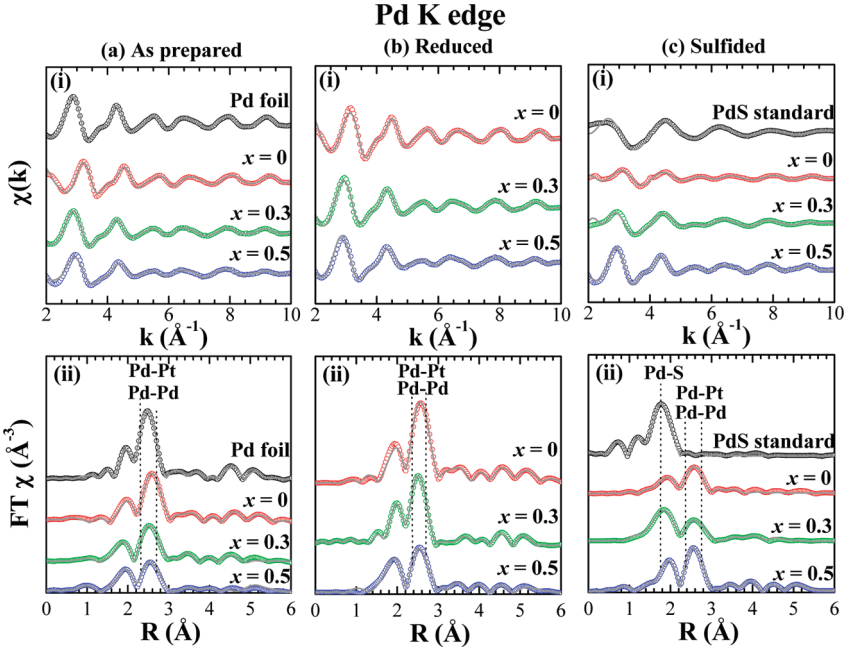

Figure 3. (i) EXAFS signals at the Pd K edge for the Pt_xPd_{1-x} nanoparticles for different x values and (ii) the corresponding FT for the (a) as prepared, (b) reduced at 300 °C, and (c) sulfided at 300 °C. The points represent the experimental data, and the gray lines are the fitting results.

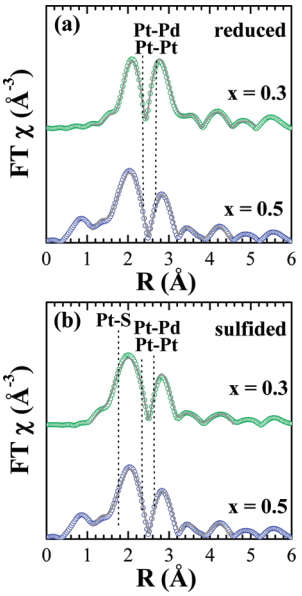

Figure 4. In situ XAS results measured at the Pt L_3 edge for the Pt_xPd_{1-x} nanoparticles. FT of the EXAFS signals for the (a) reduced at 300 °C and (b) sulfided at 300 °C. The points represent the experimental dat, a and the gray lines are the fitting results.

core.[20,29] It can be explained as follows: For the particular $x = 0.3$ case, the shell is the thicker one within the range of compositions investigated, since it has 70% of Pd atoms in the composition. There are Pt neighbors around Pd atoms only at the interface between the shell and core regions. It represents a small fraction of the total number of Pd atoms. In other words, most of the Pd atoms are surrounded by Pd (from the shell region) and S atoms (at the surface). Since the obtained coordination number of an atom is the average number of its nearest neighbors, for the proposed core−shell structure, the number of Pt atoms around Pd should be almost zero, which is consistent with the result presented in Table 3, considering the uncertainty associated in the coordination number values. On the other hand, there are 30% of Pt atoms. Then, the Pt core radius should be small and the fraction of Pt−Pd scattering (at the interface of the core−shell region) becomes important, which is consistent with the data presented in Table 1.

In order to verify the importance of the number of Pd atoms around Pt on the sulfur reactivity in a more realistic situation, in situ XAS at the Pt L_3 edge was performed just after the reduction and the sulfidation processes for $Pt_{0.5}Pd_{0.5}$ and $Pt_{0.3}Pd_{0.7}$ nanoparticles. These results are presented in Figure 4. For both samples, the sulfidation induces changes on the FT features (enlargement of the first peak) due to the formation of Pt−S bonds.

Table 4 lists the quantitative parameters obtained from the in situ measurements at the Pt L_3 edge (reduction and sulfidation at 300 °C). Typical *R*-factors were between 0.004 and 0.019, demonstrating good fit quality. The sulfur reactivity of these systems is manifested in the coordination numbers obtained for the Pt−S bond. The Pt−S pair for the $Pt_{0.5}Pd_{0.5}$ presents a coordination number 0.8 ± 0.1 at 2.23 ± 0.02 Å, and, for the $Pt_{0.3}Pd_{0.7}$ nanoparticles, it is necessary to include a Pt−S contribution with $N = 1.1 \pm 0.1$ at 2.26 ± 0.02 Å. In the ex situ XAS experiments (Table 1), the sulfided $Pt_{0.5}Pd_{0.5}$ nanoparticles do not present a Pt−S contribution, which may imply that this bond is no longer observable at room temperature measurements. The Pt−S bond parameters for the $Pt_{0.3}Pd_{0.7}$ nanoparticles coincide with the ex situ results.

Table 4. In Situ XAS Measurements at the Pt L_3 Edge: Results Obtained from the Quantitative Analysis of the EXAFS Data for the Coordination Shell Yielding the Coordination Number (N), Distance (R) and Debye Waller Factor (σ^2) for the Reduced (T = 300 °C) and Sulfided (T = 300 °C) Samples

x	pair	N	R (Å)	σ^2 (10^{-2} Å^2)
		Reduced		
0.5	Pt−Pt	5.9 ± 0.1	2.72 ± 0.02	0.72 ± 0.02
	Pt−Pd	3.3 ± 0.1	2.71 ± 0.02	0.81 ± 0.02
0.3	Pt−Pt	5.7 ± 0.2	2.74 ± 0.02	0.83 ± 0.03
	Pt−Pd	5.4 ± 0.1	2.73 ± 0.02	0.86 ± 0.02
		Sulfided		
0.5	Pt−S	0.8 ± 0.1	2.23 ± 0.02	0.40 ± 0.2
	Pt−Pt	5.0 ± 0.2	2.75 ± 0.02	0.40 ± 0.04
	Pt−Pd	2.8 ± 0.1	2.74 ± 0.02	0.51 ± 0.03
0.3	Pt−S	1.1 ± 0.1	2.26 ± 0.02	1.06 ± 0.09
	Pt−Pt	7.7 ± 0.2	2.71 ± 0.02	0.95 ± 0.02
	Pt−Pd	2.9 ± 0.1	2.71 ± 0.02	0.95 ± 0.02

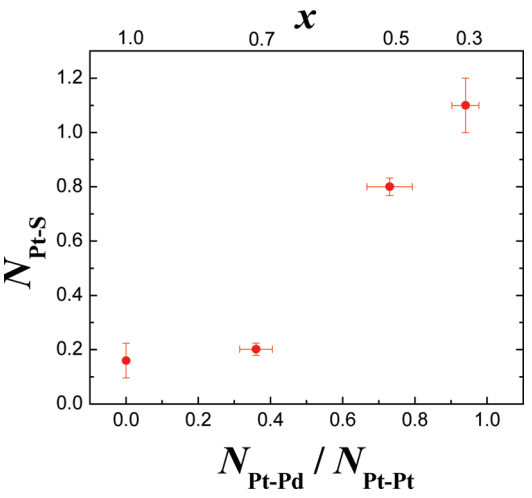

Figure 5. Relation between the coordination number N_{Pt-S} and the ratio of Pt−metal coordination numbers N_{Pt-Pd}/N_{Pt-Pt}. Data extracted from the EXAFS adjustment of the in situ measurements at the Pt L_3 edge obtained in the present and previous work.[20]

A comparison of the number of Pt−S bonds formed in terms of the nanoparticles' composition, investigated both in the present and in the previous work,[20] is displayed in Figure 5. The variation of the coordination number N_{Pt-S} is plotted as a function of the N_{Pt-Pd}/N_{Pt-Pt} ratio. The N_{Pt-Pd}/N_{Pt-Pt} values represent the relative presence of Pd with respect to Pt in the vicinity of the Pt atoms, and they were calculated from the corresponding reduced samples (also measured in situ). Therefore, these ratio values represent the atomic distribution around the absorbing Pt atoms, just prior to the exposure to sulfur. The trend observed shows that for higher N_{Pt-Pd}/N_{Pt-Pt} ratio values (and lower x values in the Pt_xPd_{1-x} nanoparticles), the number of observed Pt−S bonds is larger.

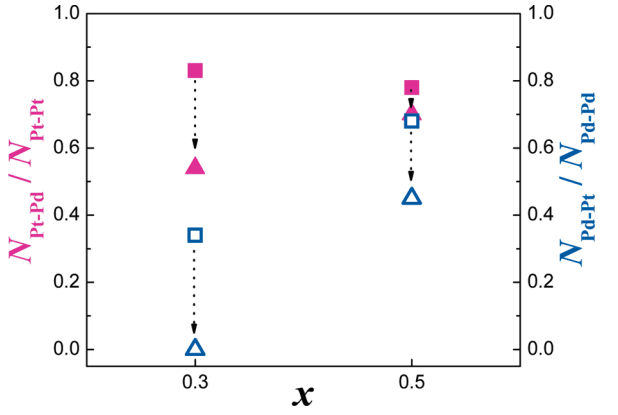

Figure 6. Relative changes in the coordination number for intermetallic with respect to the monometallic scattering contribution (N_{Pt-Pd}/N_{Pt-Pt} and N_{Pd-Pt}/N_{Pd-Pd}), before (squares) and after (triangles) the sulfidation process. Data extracted from the EXAFS adjustment of the ex situ measurements at the Pt L_3 edge and Pd K edge.

4. DISCUSSION

As in this study the atomic local structure of nonsupported nanoparticles is investigated, any interaction between the metals is unambiguously revealed.

Monometallic systems, Pd ($x = 0$) and Pt ($x = 1$),[20] have both displayed higher resistance to sulfidation when compared to the bimetallic nanoparticles. Moreover, it is clear that the number of metal−sulfur bonds increases with the increasing amount of Pd in the bimetallic systems.

These results are strong evidence that sulfur reactivity is closely related to the number of Pd atoms around Pt and, ultimately, it implies the existence of an interaction between the Pd and Pt electronic structures. If there is a charge transfer effect between Pd and Pt, it may be involved in this observation. Further investigations are planned to understand the reason for the absence of Pt−S bonds in the ex situ Pt K edge EXAFS measurements for $Pt_{0.5}Pd_{0.5}$ nanoparticles, that were observed in the in situ results of the same system.

In addition, for the bimetallic samples, the coordination number for intermetallic scattering (N_{Pt-Pd} and N_{Pd-Pt}) tends to decrease with respect to the monometallic contribution (N_{Pt-Pt} and N_{Pd-Pd}) after the sulfidation process (Figure 6). Such trend is more evident for the sample with higher Pd concentration ($x = 0.3$). In fact, for the $Pt_{0.3}Pd_{0.7}$ nanoparticles, Pd−Pt bonds are no longer observed at the Pd K edge after sulfidation. These observations corroborate the atomic rearrangement in nonsupported Pt_xPd_{1-x} nanoparticles that induces the formation of a core−shell structure, with a Pd-enriched shell and a Pt-rich core.[20,29]

Our findings are in apparent disagreement with the ones reported for supported Pt−Pd nanoparticles,[11,14,15,28] where the presence of Pd decreases the sulfur reactivity of the bimetallic system compared to monometallic (Pt). The authors suggest an electron-deficient character of the Pt atoms due to an electron transfer from Pt to the support. In addition, Pt surface segregation in the bimetallic particles was observed, which could lead to the formation of isolated Pt clusters on the Pd surface. Such structural behavior is the opposite of our case, in which the migration of Pd toward the nanoparticle's surface occurs. Such distinct atomic rearrangement observed in supported systems may explain the contradictory Pd-induced enhancement of the sulfur reactivity reported here. Despite the evidence presented here, our next step is to perform a comprehensive investigation of the electronic structure of the bimetallic nanoparticles in order to prove our model.

5. CONCLUSIONS

In summary, we have shown that the sulfur reactivity in nonsupported Pt_xPd_{1-x} nanoparticles directly depends on the amount of Pd in the bimetallic systems and increases for higher Pd content, whereas the monometallic cases presented resistance toward sulfidation. We propose that the higher reactivity is related to a modification in the electronic structure of the metals due to a charge transfer effect from the Pd to the Pt atoms in the bimetallic nanoparticles. The simultaneous formation of a (Pt-rich) core - (Pd-rich) shell structure during thermal treatments is a fundamental factor to explain the reactivity behavior of the nonsupported nanoparticles submitted to sulfidation.

AUTHOR INFORMATION

Corresponding Author

*Phone number: +55 51 33086525. Fax number: +55 51 33086510. E-mail: jonder@if.ufrgs.br.

ACKNOWLEDGMENT

We acknowledge the support given by the ELETTRA Synchrotron Light Laboratory under proposal 20085073 and LNLS (XAFS1 8179 and XAFS1 8766 proposals). TEM measurements were performed at the CME-UFRGS, and work was funded by CNPq (Brazil). The authors thank Dr. Laura Sordelli for fruitful discussions. F.B. thanks CNPq for his Ph.D. fellowship. The authors thank Dr. Laura Sordelli for fruitful discussions. We thank D.O. Silva and Professor J. Dupont for providing the samples. F.B. thanks CNPq for his Ph.D. fellowship.

REFERENCES

(1) Barbier, J.; Lamy-Pitarra, E.; Marecot, P.; Boitiaux, J.; Cosyns, J.; Verna, F. *Adv. Catal.* **1990**, *37*, 279.

(2) Navarro, R.; Pawelec, B.; Trejo, J.; Mariscal, R.; Fierro, J. Hydrogenation of aromatics on sulfur-resistant PtPd bimetallic catalysts. *J. Catal.* **2000**, *189* (1), 184–194.

(3) Jiang, H.; Yang, H.; Hawkins, R.; Ring, Z. Effect of palladium on sulfur resistance in Pt−Pd bimetallic catalysts. *Catal. Today* **2007**, *125* (3−4), 282–290.

(4) Badano, J.; Quiroga, M.; Betti, C.; Vera, C.; Canavese, S.; Coloma-Pascual, F. Resistance to sulfur and oxygenated compounds of supported Pd, Pt, Rh, Ru catalysts. *Catal. Lett.* **2010**, *137* (1), 35–44.

(5) Chang, J.; Chang, S. Catalytic properties of γ-alumina-supported Pt catalysts for tetralin hydrogenation* 1: Effects of sulfur-poisoning and hydrogen reactivation. *J. Catal.* **1998**, *176* (1), 42–51.

(6) Yasuda, H.; Yoshimura, Y. Hydrogenation of tetralin over zeolite-supported Pd−Pt catalysts in the presence of dibenzothiophene. *Catal. Lett.* **1997**, *46* (1), 43–48.

(7) Matsubayashi, N.; Yasuda, H.; Imamura, M.; Yoshimura, Y. EXAFS study on Pd−Pt catalyst supported on USY zeolite. *Catal. Today* **1998**, *45* (1−4), 375–380.

(8) Cooper, B.; Donnis, B. Aromatic saturation of distillates: An overview. *Appl. Catal. A: General* **1996**, *137* (2), 203–223.

(9) Betta, R. A. D.; Boudart, M.; Gallezot, P.; Weber, R. S. Reply to the comments of P. H. Lewis "Net charge on platinum cluster incorporated in Y zeolite". *J. Catal.* **1981**, *69* (2), 514–515.

(10) Homeyer, S. T.; Sachtler, W. M. H. Design of Metal Clusters in Nay Zeolite. In *Studies in Surface Science and Catalysis*, Jacobs, P. A.; van Santen, R. A., Eds.; Elsevier: Amsterdam/Oxford/New York, 1989; Vol. 49, pp 975−984.

(11) Yoshimura, Y.; Toba, M.; Matsui, T.; Harada, M.; Ichihashi, Y.; Bando, K.; Yasuda, H.; Ishihara, H.; Morita, Y.; Kameoka, T. Active phases and sulfur tolerance of bimetallic Pd−Pt catalysts used for hydrotreatment. *Appl. Catal. A: Gen.* **2007**, *322*, 152–171.

(12) Roucoux, A.; Schulz, J.; Patin, H. Reduced transition metal colloids: A novel family of reusable catalysts?. *Chem. Rev.* **2002**, *102* (10), 3757–3778.

(13) Sinfelt, J. H. Supported "bimetallic cluster" catalysts. *J. Catal.* **1973**, *29* (2), 308–315.

(14) Rousset, J.; Stievano, L.; Cadete Santos Aires, F.; Geantet, C.; Renouprez, A.; Pellarin, M. Hydrogenation of tetralin in the presence of sulfur over γ-Al_2O_3-supported Pt, Pd, and Pd−Pt model catalysts. *J. Catal.* **2001**, *202* (1), 163–168.

(15) Lin, T.; Jan, C.; Chang, J. Aromatics reduction over supported platinum catalysts. 2. Improvement in sulfur resistance by addition of palladium to supported platinum catalysts. *Ind. Eng. Chem. Res.* **1995**, *34* (12), 4284–4289.

(16) Gallezot, P.; Alarcon-Diaz, A.; Dalmon, J. A.; Renouprez, A. J.; Imelik, B. Location and dispersion of platinum in PtY zeolites. *J. Catal.* **1975**, *39* (3), 334–349.

(17) Markovic, N. M.; Ross, P. N. Surface science studies of model fuel cell electrocatalysts. *Surf. Sci. Rep.* **2002**, *45* (4−6), 117–229.

(18) Matsui, T.; Harada, M.; Ichihashi, Y.; Bando, K. K.; Matsubayashi, N.; Toba, M.; Yoshimura, Y. Effect of noble metal particle size on the sulfur tolerance of monometallic Pd and Pt catalysts supported on high-silica USY zeolite. *Applied Catalysis A: General* **2005**, *286* (2), 249–257.

(19) Yasuda, H.; Matsubayashi, N.; Sato, T.; Yoshimura, Y. Confirmation of sulfur tolerance of bimetallic Pd−Pt supported on highly acidic USY zeolite by EXAFS. *Catal. Lett.* **1998**, *54* (1), 23–27.

(20) Bernardi, F.; Alves, M. C. M.; Traverse, A.; Silva, D.; Scheeren, C.; Dupont, J.; Morais, J. Monitoring atomic rearrangement in $Pt_x Pd_{1-x}$ (x = 1, 0.7, or 0.5) nanoparticles driven by reduction and sulfidation processes. *J. Phys. Chem. C* **2009**, *113* (10), 3909–3916.

(21) Scheeren, C. W.; Machado, G.; Teixeira, S. R.; Morais, J.; Domingos, J. B.; Dupont, J. Synthesis and characterization of Pt(0) nanoparticles in imidazolium ionic liquids. *J. Phys. Chem. B* **2006**, *110* (26), 13011–13020.

(22) Bernardi, F.; Alves, M. C. M.; Scheeren, C. W.; Dupont, J.; Morais, J. In situ studies of nanoparticles under reaction with sulfur by XAS. *J. Electron Spectrosc. Relat. Phenom.* **2007**, *156−158*, 186–190.

(23) Tolentino, H.; Ramos, A.; Alves, M.; Barrea, R.; Tamura, E.; Cezar, J.; Watanabe, N. A 2.3 to 25 keV XAS beamline at LNLS. *J. Synchrotron Radiat.* **2001**, *8* (3), 1040–1046.

(24) Koningsberger, D.; Prins, R. *X-ray Absorption: Principles, Applications and Techniques of EXAFS, SEXAFS and XANES in Chemical Analysis*; John Wiley & Sons: New York, 1988; Vol. 92.

(25) Newville, M. IFEFFIT: Interactive XAFS analysis and FEFF fitting. *J. Synchrotron Radiat.* **2001**, *8* (2), 322–324.

(26) Zabinsky, S. I.; Rehr, J. J.; Ankudinov, A.; Albers, R. C.; Eller, M. J. Multiple-scattering calculations of X-ray-absorption spectra. *Phys. Rev. B* **1995**, *52* (4), 2995.

(27) Greegor, R. B.; Lytle, F. W. Morphology of supported metal clusters: Determination by EXAFS and chemisorption. *J. Catal.* **1980**, *63* (2), 476–486.

(28) Guillon, E.; Lynch, J.; Uzio, D.; Didillon, B. Characterisation of bimetallic platinum systems: Application to the reduction of aromatics in presence of sulfur. *Catal. Today* **2001**, *65* (2−4), 201–208.

(29) Bernardi, F.; Fecher, G. H.; Alves, M.; Morais, J. Unraveling the formation of core−shell structures in nanoparticles by S-XPS. *J. Phys. Chem. Lett.* **2010**, *1*, 912–917.